prepared at 1000°C rapidly reached saturation and displayed room-temperature hysteresis (with a small remanence) in its magnetization, as shown in Fig. 5D. This is characteristic of a ceramic material in which the $Fe_n$ clusters have become just large enough to display ferromagnetism. Thus, in ceramics prepared below 900°C, the iron nanoclusters are superparamagnetic, whereas ceramics prepared at higher temperatures contain larger iron clusters that are ferromagnetic. By varying the pyrolysis temperature and time of the polymer precursor, we can control the magnetic properties of the resulting ceramic.

Nanoindentation measurements provided values of the Young's modulus $E$ for the superparamagnetic ceramic formed at 850°C (29.4 GPa) and the ferromagnetic ceramic formed at 1000°C (15.4 GPa). For comparison, the Young's modulus for the polymer precursor CPPN was $E = 6.9$ GPa. The values for the magnetic ceramics are greater than that of graphite ($E = 4.8$ GPa) and are in the same region as that of borosilicate glass ($E = 17.5$ GPa) (*25*).

This report illustrates a metal-containing organosilicon polymer network that functions as a controlled iron delivery vehicle and as a matrix for the nucleation and growth of iron nanoclusters. The ceramics can be molded into shapes and may exhibit interesting magnetic, electrical, and optical properties.

**References and Notes**


1. H.-P. Baldus and M. Jansen, *Angew. Chem. Int. Ed. Engl.* **36**, 328 (1997).
2. J. Bill and F. Aldinger, *Adv. Mater.* **7**, 775 (1995).
3. D. Segal, *Chemical Synthesis of Advanced Ceramic Materials* (Cambridge Univ. Press, New York, 1991).
4. M. Peuckert, T. Vaahs, M. Brück, *Adv. Mater.* **2**, 398 (1990).
5. R. M. Laine and F. Babonneau, *Chem. Mater.* **5**, 260 (1993).
6. T. Wideman, E. E. Remsen, E. Cortez, V. L. Chlanda, L. G. Sneddon, *Chem. Mater.* **10**, 412 (1998).
7. G. T. Visscher, D. C. Nesting, J. V. Badding, P. A. Bianconi, *Science* **260**, 1496 (1993).
8. J. He, M. Scarlete, J. F. Harrod, *J. Am. Ceram. Soc.* **78**, 3009 (1995).
9. S. Bourg, B. Boury, R. J. P. Corriu, *J. Mater. Chem.* **8**, 1001 (1998).
10. E. J. Houser and T. M. Keller, *Macromolecules* **31**, 4038 (1998).
11. Q. Liu, W. Shi, F. Babonneau, L. V. Interrante, *Chem. Mater.* **9**, 2434 (1997).
12. S. Yajima and M. Omori, *Nature* **267**, 823 (1977).
13. D. Thompson, *Nature* **389**, 675 (1997).
14. R. Riedel *et al.*, *Nature* **382**, 796 (1996).
15. I. Manners, *Angew. Chem. Int. Ed. Engl.* **35**, 1602 (1996).
16. D. A. Foucher, B.-Z. Tang, I. Manners, *J. Am. Chem. Soc.* **114**, 6246 (1992).
17. I. Manners, *Chem. Commun.* **1999**, 857 (1999).
18. _____, *Can. J. Chem.* **76**, 371 (1998).
19. R. Petersen *et al.*, *Chem. Mater.* **7**, 2045 (1995).
20. M. J. MacLachlan, P. Aroca, N. Coombs, I. Manners, G. A. Ozin, *Adv. Mater.* **10**, 144 (1998).
21. M. J. MacLachlan, A. J. Lough, W. E. Geiger, I. Manners, *Organometallics* **17**, 1873 (1998).
22. The ceramics exhibiting shape retention were obtained as follows. A Pyrex glass tube was loaded with 2.2 g (8.7 mmol) of SSFP and sealed under vacuum. The sample was heated for 7 hours at 150°C, followed by 16 hours at 180°C. After cooling to room temperature, the tube was broken open to give a rigid, cylindrical sample of CPPN that replicated the shape of the Pyrex polymerization tube. The sample was stirred in THF for 24 hours, but virtually no material dissolved. Next, a section of the orange-red shaped ceramic precursor (1.506 g) was dried under vacuum and then placed in a quartz boat inside a tube furnace. The sample was heated to 600°C over 4 hours and maintained at that temperature for 1 hour under a gentle flow of nitrogen (about 10 ml $min^{-1}$). A black, lustrous ceramic that appeared identical in shape to the precursor was obtained (1.351 g, 90% yield). Ceramics were also prepared at higher temperatures (every 50°C up to 1000°C) under similar conditions. Yields of 90 ± 2% were obtained in each case.
23. L. M. Epstein, *J. Chem. Phys.* **36**, 2731 (1962).
24. We have studied the genesis of the ceramic in great detail using a multianalytical diffraction, microscopy, spectroscopy and thermal analysis approach, over the temperature range 25° to 1000°C. Full details of this study will be published later. For reference purposes, key data are included in supplementary material (available at www.sciencemag.org/feature/data/1047398.shl).
25. J. F. Shackelford, W. Alexander, J. S. Park, Eds., *CRC Materials Science and Engineering Handbook* (CRC Press, Boca Raton, FL, ed. 2, 1994), p.514.


26. We acknowledge C. Berry for gas adsorption measurements and G. Favoro for nanoindentation measurements. We thank the Natural Sciences and Engineering Research Council (NSERC) of Canada for financial support. The Mössbauer data provided by C. Jones are appreciated. M.J.M. thanks NSERC for a postgraduate scholarship (1995–99). I.M. thanks the Ontario Government for a PREA Award (1999–2004), NSERC for an E. W. R. Steacie Fellowship (1997–99), and the University of Toronto for a McLean Fellowship (1997–2003). G.A.O. thanks the Killam Foundation for an Isaac Walton Killam Foundation Fellowship (1995–97).

26 November 1999; accepted 5 January 2000


# Superplastic Extensibility of Nanocrystalline Copper at Room Temperature


**L. Lu,[1] M. L. Sui,[2] K. Lu[1]***



**A bulk nanocrystalline (nc) pure copper with high purity and high density was synthesized by electrodeposition. An extreme extensibility (elongation exceeds 5000%) without a strain hardening effect was observed when the nc copper specimen was rolled at room temperature. Microstructure analysis suggests that the superplastic extensibility of the nc copper originates from a deformation mechanism dominated by grain boundary activities rather than lattice dislocation, which is also supported by tensile creep studies at room temperature. This behavior demonstrates new possibilities for scientific and technological advancements with nc materials.**


Plastic deformation in polycrystalline solids occurs by movement of lattice dislocations and/or diffusional creep. The dislocation movement mechanism predominates in most conventional materials at relatively low temperatures when atomic diffusivity is minor. A strain-hardening effect is always associated with this mechanism, which arises from the pileup of lattice dislocations blocked at grain boundaries. The strain-hardening effect often restricts the mechanical processing of metals, which must be eliminated by thermal annealing in order to perform further deformation without crack formation. Plastic deformation occurs at higher temperatures when atomic diffusivity is considerably increased (at grain boundaries or inside the lattice); in this case, diffusion creep becomes a dominant mechanism. The diffusion creep rate ($\dot{\varepsilon}$), which is dominated by grain boundary diffusion, is related to grain size by (*1*)

$$\dot{\varepsilon} = \frac{B\Omega\sigma\delta D_{gb}}{d^3 kT}$$

where $\sigma$ is tensile stress, $\Omega$ is atomic volume, $d$ is average grain size, $B$ is a numerical constant, $D_{gb}$ is grain boundary diffusivity, $\delta$ is grain boundary thickness, and $k$ is Boltzmann's constant. This relation suggests that diffusional creep may be enhanced when grain size is reduced and/or grain boundary diffusivity is enhanced. Based on this mechanism, a decade ago Gleiter *et al.* (*2, 3*) predicted that a nanocrystalline (nc) material, one in which the crystallite size is in the nanometer regime, would make it amenable to high creep rates and large-scale deformation at much lower homologous temperatures, so that ductile ceramics and diffusional creep of pure metals would be possible even at room temperature (*3*). This possibility is of great interest because not only may it shed light on the deformation mechanism of the nanostructure, but it also may significantly facilitate the fabrication process for producing components with complex shapes. Such


[1]State Key Laboratory for Rapidly Solidified Nonequilibrium Alloys, [2]Laboratory for Atomic Imaging of Solids, Institute of Metal Research, Chinese Academy of Sciences, Shenyang 110015, People's Republic of China.

*To whom correspondence should be addressed. E-mail: kelu@imr.ac.cn

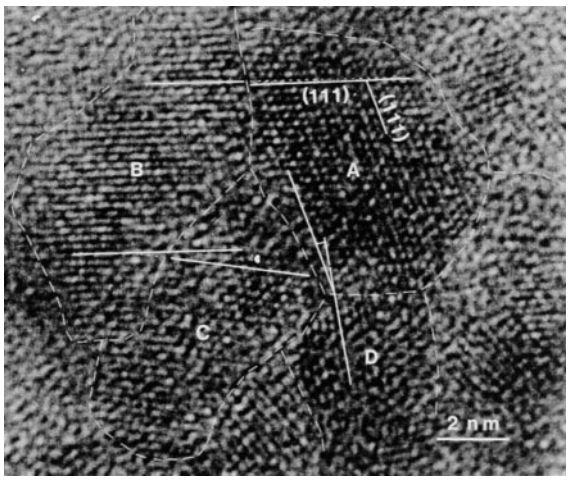


**Fig. 1.** HRTEM observation of a few nanocrystallites in the as-deposited nc Cu sample. Four crystallites (A, B, C, and D) are outlined by dashed white lines. The orientation difference angle of (111) plan between A and B is about 1°, that between B and C is about 9°, and that between A and D is about 10°. Most nanocrystallites in the as-deposited sample are separated by the small-angle (1° to 10°) grain boundaries.

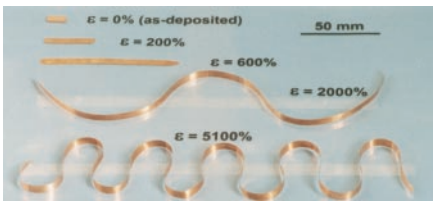


**Fig. 2.** The nc Cu specimens before and after cold rolling at room temperature with different amounts of deformation degree ($\varepsilon$) as indicated.

expectations are supported by recent computer simulation results, which indicate that plastic deformation of nc metals occurs by grain boundary sliding and motion, with minor lattice dislocation activity (*4, 5*). The observed deformation mode is in some ways similar to the way grain boundaries carry most of the deformation in superplasticity (*6*). A softening with grain size (decreasing) in nc Cu is also seen in the simulation as a result of the dominant grain boundary deformation mechanism (*4*).

However, recent experimental observations are disappointing: Most nc metal samples are very brittle, with little tensile ductility and an extremely small diffusional creep rate at room temperature (*7–9*). Although softening of nc metals was detected from hardness measurements in several metal and alloy systems, directly measured creep rates in the consolidated nc metals at room temperature are normally two to four orders of magnitude smaller than the expected values (*10*). Depression in superplastic temperatures recently has been observed in some nc metals and alloys (*11*), but the expected room-temperature superplasticity in nc metals has not been observed until now. Many of these disappointing experimental results can be attributed to artifacts, which are present in nc samples that were induced during sample processing procedures, such as imperfect bonding and/or porosity, contamination, and large microstrain. To eliminate these factors, which influence the deformation behavior and reveal the intrinsic mechanical properties of nc metals, "ideal" nc samples are urgently needed—that is, samples with pure (free of contamination) and dense (perfect bonding of crystallites and porosity-free) nc samples with a minimized defect density (microstrain).

Among the various synthesis methods of nc materials, electrodeposition is one of the effective approaches for producing porosity-free nc metals with a small microstrain (*12*). In this study, a nc pure Cu (purity better than 99.993 atomic % and a total oxygen content of about 24 ± 1 parts per million) was prepared by an electrodeposition technique with an electrolyte of $CuSO_4$ and a Ti substrate. The sample density is 8.91 ± 0.03 g/cm$^3$, or 99.4% of the theoretical density of Cu. Positron annihilation spectroscopy measurements verified the high density and indicated no vacancy-cluster–like volumes or missing crystallites (pores) existing in the as-deposited sample. The average grain size determined from x-ray diffraction (XRD) analysis in terms of diffraction line broadening of seven single Bragg reflection peaks [by the Wilson method (*13*)] is about 28 nm. The microstrain in the as-deposited sample determined by XRD is only 0.03%, which is about one order of magnitude lower than that in the ball-milled and consolidated nc metals. Microstructure characterization by means of high-resolution transmission electron microscopy (HRTEM) observation indicated that the as-deposited sample consists of ultrafine crystallites (or crystalline domains) with sizes ranging from a few nanometers to about 80 nm. The average grain size is about 20 nm, which is close to the XRD result. Most of the nanometer-sized crystallites are equiaxed and separated by small-angle grain boundaries that consist of dislocation arrays, in contrast to the conventional large-angle grain boundaries in consolidated and ball-milled nc metals. Figure 1 shows a typical HRTEM observation of a few nanocrystallites; between them are small-angle (1° to 10°) grain boundaries.

Plastic deformation of the as-deposited nc Cu specimen was done by cold rolling at room temperature. A piece of the nc Cu sample (16 × 4 × 1 mm) cut from the as-deposited sheet was rolled at room temperature with a twin-roller (diameter, 40 mm) apparatus. The strain rate during rolling was controlled to be around $1 \times 10^{-3}$ to $1 \times 10^{-2}$ s$^{-1}$. Cold rolling resulted in a continuous increase in the sample length in the direction of rolling, while the sample width was kept unchanged. After repeated rolling, the nc Cu sample became a strip with no cracks forming at the sample edges. With the progress of repeated rolling, the sample became longer and longer, as shown in Fig. 2, and eventually resulted in a uniform, long thin ribbon (about 20 μm thick) with smooth surfaces and straight edges. The total degree of deformation, $\epsilon = (t_0 - t)/t$, in our samples (where $t_0$ and $t$ denote thickness of the initial and the as-rolled samples, respectively) can be as large as 5100%. Further cold rolling is still possible to extend the deformation. Such extreme extensibility of the nc Cu sample has not been observed in the conventional coarse-grained polycrystalline Cu, which typically would break after extensions of 800%.

The nc Cu was annealed at 500°C for 48 hours in a vacuum, which resulted in a much larger grain size of about 100 μm. The as-annealed Cu sample was rolled under the same circumstances. It was found that, when the deformation degree reaches about 700%, the sample is remarkably hardened and cracks are formed at sample edges, as usually observed for conventional coarse-grained Cu. This observation implies that the extreme extensibility in the as-deposited Cu originates from the ultrafine-grained structures, and other effects, including the purity effect, can be ruled out.

Microhardness measurements showed a slight hardness increase in the as-deposited nc Cu induced at the initial stage of rolling, from 1.05 GPa (as-deposited) to 1.20 GPa ($\varepsilon$ = 800%), as shown in Fig. 3, and no strain hardening effect was seen with further rolling ($\varepsilon >$ 800%). This result contrasts with the evident strain hardening effect in conventional coarse-grained Cu from 0.6 GPa (initial state) to 1.57 GPa ($\varepsilon$ = 800%, with crack formation), and in the as-annealed Cu from 0.51 GPa (initial state) to 1.45 GPa ($\varepsilon$ = 650%, with crack formation), also in Fig. 3, respectively. The hardness variation tendencies differ fundamentally between the nc and the coarse-grained Cu samples, which indicates different underlying deformation mechanisms.

HRTEM observations showed that, in the as-rolled nc Cu samples with a deformation degree of 4800%, there is no obvious grain size difference as in the as-deposited nc Cu

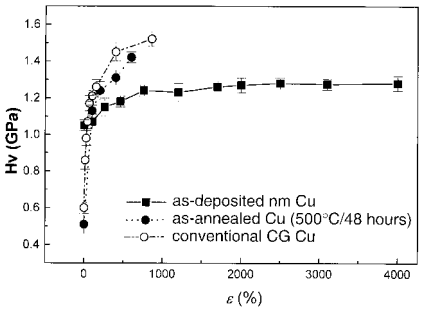


**Fig. 3.** Microhardness variation with deformation degree of cold rolling for the as-deposited nc Cu specimen, the conventional coarse-grained polycrystalline Cu, and the as-annealed coarse-grained Cu as indicated. Cracks were formed at sample edges when $\varepsilon \approx 800\%$ for the coarse-grained Cu sample.

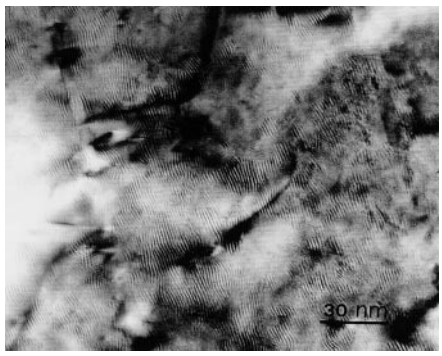


**Fig. 4.** HRTEM observation of the as-rolled nc Cu sample with a deformation degree of 4800%.

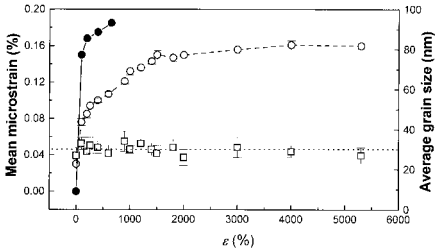


**Fig. 5.** XRD measurement results of the microstrain (open circles) and the average grain size (open squares) for the nc Cu samples and the microstrain for the as-annealed coarse-grained Cu sample (solid circles) as a function of deformation degree of cold rolling.

sample, and the crystallites are still roughly equiaxed. However, the dislocation density (mainly located at grain boundaries) in the as-rolled specimens increased, which led to an evident increase in the grain boundary misorientation angles between the nanocrystallites, as shown in Fig. 4. The misorientation between neighboring Cu nanocrystallites can be estimated from the observed moiré finger modulations. We found that, for the cold-rolled nc sample, the misorientation angle of the nanocrystallites ranges from about 6° to 18°, which is evidently larger than that for the as-deposited sample (1° to 10°). That means the nanocrystallites (or domains) separated by small-angle grain boundaries in the as-deposited nc Cu may transform into grains (or domains) with increased misorientations during the cold-rolling process. Quantitative XRD measurements confirmed that the average grain size of the nc Cu remained unchanged during rolling, whereas the microstrain (which is a signature of the defect/dislocation density) increased in the initial stage ($\varepsilon < 1000\%$) and tended to saturate at a value of about 0.16% when $\varepsilon \geq 1000\%$ (see Fig. 5). Such variation of microstrain in the nc Cu shows a completely different behavior from that of the as-annealed coarse-grained Cu (Fig. 5).

The variation tendency of microstrain agrees very well with the hardness measurement results, indicating that when the as-deposited nc Cu is rolled, a minor dislocation activity (generation and movement) may occur in the initial stage, presumably in large grains, that corresponds to a slight increment in hardness. This phenomenon was observed in computer simulations of the deformation in a nc Cu (*4*). Further deformation results in saturation of the lattice dislocating density when the dislocation generation and annihilation are compensated. As soon as the large-angle grain boundary grains are formed, plastic deformation might be carried predominantly by grain boundary activities, such as grain boundary sliding or slip, as seen in other nc materials (*14*). The constant grain size, constant dislocation density, and constant hardness confirmed that plastic deformation of the nc Cu is dominated by the grain boundary mechanism instead of by dislocation activities.

Tensile creep measurements around room temperature [0.22 to 0.24 melting temperature ($T_m$)] were performed with the as-deposited nc Cu (*15*). We find evidence of obvious creep near room temperature with threshold stress $\sigma_0$ that decreases with increasing temperature. The steady state creep rate at 0.23 $T_m$ was measured to be as large as $1 \times 10^{-6}$ $s^{-1}$, which is much larger than that for coarse-grained Cu and the consolidated nc Cu ($8 \times 10^{-9}$ $s^{-1}$) (*10*) as well. The creep rates increased linearly with an increasing applied stress: $d\varepsilon/dt = 2.51 \times 10^{-14}\,\sigma$ (where $\sigma$ is in Pa and $d\varepsilon/dt$ is in $s^{-1}$) at 303 K in the as-deposited nc Cu sample. Following the creep rate equation dominated by grain boundary diffusion (i.e., the Coble creep), the predicted value of the creep rate is $d\varepsilon/dt = 1.65 \times 10^{-12}\,\sigma$ at 303 K when the diffusivity ($D_{gb}$) value is taken from a consolidated nc Cu (*16*). When the diffusivity for the conventional grain boundary was applied, a smaller creep rate was obtained: $d\varepsilon/dt = 1.63 \times 10^{-13}\,\sigma$. This value agrees with our observed creep rate in the present nc Cu when the special (small-angle) grain boundary in our sample is taken into account.

However, even though the observed deformation behavior in this sample can be qualitatively or semiquantitatively interpreted by the grain boundary diffusion creep model, other possible deformation mechanisms could not be ruled out at this stage—for example, the grain boundary sliding model based on the rate-limiting step of deformations (*17*). The intrinsic deformation mechanism for the nc Cu sample should be clarified by more quantitative experimental results and theoretical analysis.

Our success in obtaining such superplastic extensibility at room temperature in the nc Cu sample might be attributed to the minimal artifacts in the nc sample. The high purity and full density of this nc Cu eliminated the effects of contamination and imperfect bonding (or porosity), which normally exist in consolidated nc specimens and which are effective in restricting the movement of grain boundaries and hence resisting deformation. High-angle random grain boundaries may slide more readily than the small-angle boundaries or special, such as low $\sigma$, boundaries. However, as seen in the present nc Cu, creep behavior around room temperature is evident. It indicates that the small-angle grain boundaries remain effective in carrying out large deformations at room temperature when the grain size is ultrafine, as the creep rate is proportional to $d^{-3}$. It is also seen that, when the deformation degree exceeds 1000%, with which the grain boundary misorientation has been increased, the grain boundary sliding or slip became more predominant in deformation and no strain hardening effect was detected.

The traditional deformation-annealing-deformation technique that is routinely used for deforming metals may be much simplified by using nc metals as starting materials. With proper post-heat treatments to the deformed nc metals, the microstructure of the metal may be easily controlled by optimizing the grain growth kinetics so that novel properties and behaviors in the final products can be achieved. Such an innovative material processing technique by means of superplastic deformation of nc metals will be useful in modern industry in fields such as micromachining, nanotechnology, and electronics.

### References and Notes

1. R. L. Coble, *J. Appl. Phys.* **34**, 1679 (1963).
2. J. Karch, R. Birringer, H. Gleiter, *Nature* **330**, 556 (1987).
3. A. H. Chokshi, A. Rosen, J. Karch, H. Gleiter, *Scr. Metall.* **23**, 1679 (1989).
4. J. Schiotz, F. D. Di Tolla, K. W. Jacobsen, *Nature* **391**, 561 (1998).
5. H. Van Swygenhoven and A. Caro, *Appl. Phys. Lett.* **71**, 1652 (1997).
6. A. K. Mukherjee, in *Materials Science and Technology Vol. 6, Plastic Deformation and Fracture of Materials*, H. Mughrabi, Ed. (VCH, Verlagsgesellschaft, Weinheim, Germany, 1993), chap. 9.
7. C. C. Koch, D. G. Morris, K. Lu, A. Inoue, *Mater. Res. Soc. Bull.* **24**, 54 (1999).
8. P. G. Sanders, J. A. Eastman, J. R. Weertman, in

*Processing and Properties of Nanocrystalline Materials*, C. Suryanarayana, J. Singh, F. H. Froes, Eds. (TMS, Warrendale, PA, 1996), p. 379.
9. N. Wang, Z. R. Wang, K. Aust, U. Erb, *Mater. Sci. Eng.* **A237**, 150 (1997).
10. P. G. Sanders *et al.*, *Nanostruct. Mater.* **9**, 433 (1997).
11. S. X. McFadden *et al.*, *Nature* **398**, 684 (1999).
12. U. Erb, A. M. El-Sherik, G. Palumbo, K. T. Aust, *Nanostruct. Mater.* **2**, 383 (1993).
13. H. P. Klug and L. E. Alexander, *X-Ray Diffraction Procedures for Polycrystalline and Amorphous Materials* (Wiley, New York, 1974), p. 618.
14. R. S. Mishra, S. X. McFadden, A. K. Mukherjee, *Mater. Sci. Forum Vols.* **304**, 31 (1999).
15. B. Cai, Q. P. Kong, L. Lu, K. Lu, *Scr. Metall.* **41**, 755 (1999).
16. J. Horvath, R. Birringer, H. Gleiter, *Solid State Comm.* **62**, 391 (1987).
17. H. Hahn, P. Mondal, K. A. Padmanabhan, *Nanostruct. Mater.* **9**, 603 (1997).
18. Supported by the Chinese Academy of Sciences, the National Science Foundation of China (grants 59431021 and 59625101), and the Ministry of Sciences and Technology of China (grant G1999064505). The authors thank S. L. Gu for his assistance in sample preparation.

13 October 1999; accepted 21 December 1999

# Room Temperature Magnetic Quantum Cellular Automata

**R. P. Cowburn* and M. E. Welland**

**All computers process information electronically. A processing method based on magnetism is reported here, in which networks of interacting submicrometer magnetic dots are used to perform logic operations and propagate information at room temperature. The logic states are signaled by the magnetization direction of the single-domain magnetic dots; the dots couple to their nearest neighbors through magnetostatic interactions. Magnetic solitons carry information through the networks, and an applied oscillating magnetic field feeds energy into the system and serves as a clock. These networks offer a several thousandfold increase in integration density and a hundredfold reduction in power dissipation over current microelectronic technology.**

The silicon microchip has been one of the most impressive feats of engineering ever performed. In the case of microprocessors, the number of transistors on a chip has steadily doubled every 18 months for the last 25 years, with a commensurate growth in information-processing capability (*1*). While there is still much potential for future growth, a point will eventually come when further increases become prohibitively difficult (*2*). At this point there may be interest in introducing a new paradigm for digital logic. Much interest has recently been focused on single electron transistors (SETs) as candidates for continuing the growth of both processors and memory beyond that of conventional silicon devices (*3*). A particularly interesting configuration of SETs called quantum cellular automata (QCA) has recently shown the ability to perform logic operations (*4*). Unfortunately, these devices only work at very low temperatures (millikelvin) unless the SET island dots are made to be extremely small (~2 nm).

We demonstrate experimentally that QCA architectures using relatively large dots (~100 nm) can be made to work at room temperature if one uses magnetic metals to make the dots.

Each QCA network (Fig. 1) consists of a single elongated input dot followed by a chain of 69 circular dots, each of diameter 110 nm, placed on a pitch of 135 nm. The dots were 10 nm thick and were made from the common magnetic alloy Supermalloy ($Ni_{80}Fe_{14}Mo_5X_1$, where X is other metals) on a single-crystal silicon substrate. The uniaxial anisotropy field in the unpatterned Supermalloy was less than 3 Oe. The dots were fabricated by high-resolution electron beam lithography in a polymethlymethacrylate resist followed by metalization and ultrasonic assisted lift-off in acetone. Further technical details of the fabrication and structural characterization of our magnetic nanostructures can be found in (*5*).

Electronic QCA is termed "quantum" because it uses quantum mechanical tunneling of charge between dots to change logic state; classical electrostatics are used thereafter to propagate the logic state. The quantum mechanical interactions in the magnetic QCA (MQCA) networks are exchange interactions between spins within a single dot in order to form a single giant classical spin (*5*). A logic 1 is signaled when the dot's magnetization vector points to the right, say, and a logic 0 when it points to the left. The magnetic field emanating from such a magnetic particle can be extremely large, with the result that one magnetic dot is strongly influenced by the magnetic field coming from its nearest neighbors. These classical magnetostatic interactions are then used to propagate information along the chain of dots (*6*). A further feature of magnetostatic interactions is that they force the magnetization to point along the length of the chain. The system is thus intrinsically binary, with only right- and left-pointing magnetization states being stable.

Elongating the shape of a dot introduces shape anisotropy, which greatly increases its switching field. Such a dot is still able to influence neighboring circular dots but is itself unaffected by them. We therefore use elongated dots to inject signals into the network. We set the state of the input dots by an external pulsed magnetic field applied to the entire network. Once set, the shape anisotropy of the input dots ensures that their magnetization state is preserved until the next field pulse.

We choose for simplicity to probe the magnetic state of the MQCA networks by a magneto-optical measurement (*7*). A linearly polarized laser beam is focused onto the networks, and the polarization state of the reflected light is measured in order to access the longitudinal Kerr effect (*8*). The plane of incidence of the light is set to lie along the length of the chains. The focused laser spot covers almost the entire 9-μm length of the networks, and so the recorded signal is a measure of the total component of magnetization lying along the chain of dots and, once

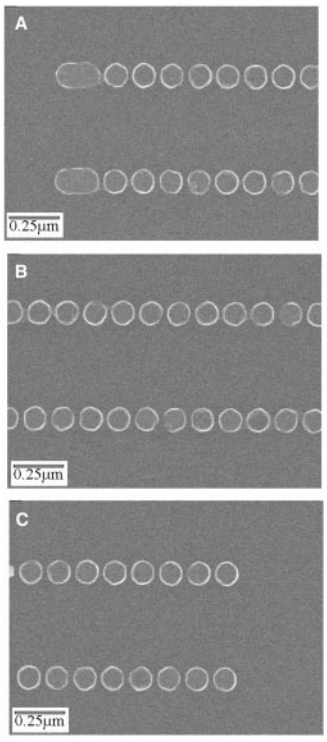


**Fig. 1.** Scanning electron micrographs of the left (**A**), center (**B**), and right (**C**) regions of two of the room temperature MQCA networks that we have fabricated.

Nanoscale Science Laboratory, Department of Engineering, University of Cambridge, Trumpington Street, Cambridge CB2 1PZ, UK.

*To whom correspondence should be addressed. E-mail: rpc12@cam.ac.uk